nature communications

Article

https://doi.org/10.1038/s41467-026-70770-z

Photoresist-guided indirect photopatterning of quantum dots via carbene-mediated ligand thermocrosslinking

Received: 2 February 2024

Accepted: 2 March 2026

Published online: 19 March 2026

Check for updates

Hyeokjun Kim[1,8], Hyobin Ham[2,8], Chang Hyeok Lim[1,8], Jin Su Park[3], SeungHwan Roh[1], Hak June Lee[3], Myeongjae Lee[2], Jinho Keum[1], Se Young Park[1], Jeong Woo Park[3], Seongjae Lee[1], Hajin Bhang[1], Seunghan Lee[1], Hyunwoo Jo[1], Yong Hyun Jo[1], Jin-Wook Shin[4], Wan Ki Bae[3], Chan-mo Kang[4] ✉, Moon Sung Kang[1,5] ✉ & BongSoo Kim[2,6,7] ✉

Colloidal quantum dots (QDs) are leading candidates for next-generation optoelectronics owing to their tuneable bandgaps, narrow emission linewidths, and high luminescence quantum yields. For virtual-, augmented-, and mixed-reality display applications of these materials, patterning full-color QDs at μm-length scales is essential. However, existing photolithographic approaches often degrade QD luminance characteristics by exposing them to harsh processing conditions, or they compromise the structural fidelity of the resulting patterns. Here we report a photoresist-guided indirect (PIN) photopatterning strategy that includes (i) lithographic formation of sacrificial PR patterns, (ii) deposition of a crosslinked QD film on top, and (iii) PR stripping that removes the sacrificial PR, leaving behind crosslinked QD patterns on the substrate. QD crosslinking is mediated by a diazo-based ligand thermocrosslinker, Diazo-4-LiXer. Leveraging low-temperature (110–120 °C)-activated carbene chemistry, Diazo-4-LiXer bridges neighbouring QDs while maintaining their intrinsic photoluminescence and electroluminescence through repeated processing. Moreover, Diazo-4-LiXer enables thermocrosslinking without affecting the underlying photoresist pre-patterns, which serve as structural templates determining the thickness and fidelity of the QD patterns. Using PIN photopatterning, we realize high-fidelity RGB patterns exceeding 4,000 pixels per inch resolution and demonstrate integration-level scalability by fabricating a 10 × 10 passive-matrix full-colour RGB QD–LED array.

Displays present digital images, acting as interfaces between human eyes and electronic signals. While conventional displays such as television, monitors, tablets, and smartphones dominate the market, there is a rapidly growing demand for head-mounted displays (HMDs) for powering virtual-reality (VR), augmented-reality (AR), and mixed-reality (MR) experiences. Given the short distance between HMDs and human eyes, the size of these displays is typically limited to a few inches in diagonal (Fig. 1a)[1,2]. This limited screen size introduces a challenge called the screen-door effect because subpixel boundaries become noticeable and affect visual quality[3]. To avoid the screen-door effect, it is essential to fabricate HMDs with ultra-high pixel densities exceeding 3000 pixels per inch (PPI), where subpixels are separated by only a few micrometers[4]. Achieving such high pixel densities is pivotal not only for eliminating the screen-door effect but also for reducing

A full list of affiliations appears at the end of the paper. ✉e-mail: nkcm@etri.re.kr; kangms@sogang.ac.kr; bongsoo@unist.ac.kr

https://doi.org/10.1038/s41467-026-70770-z

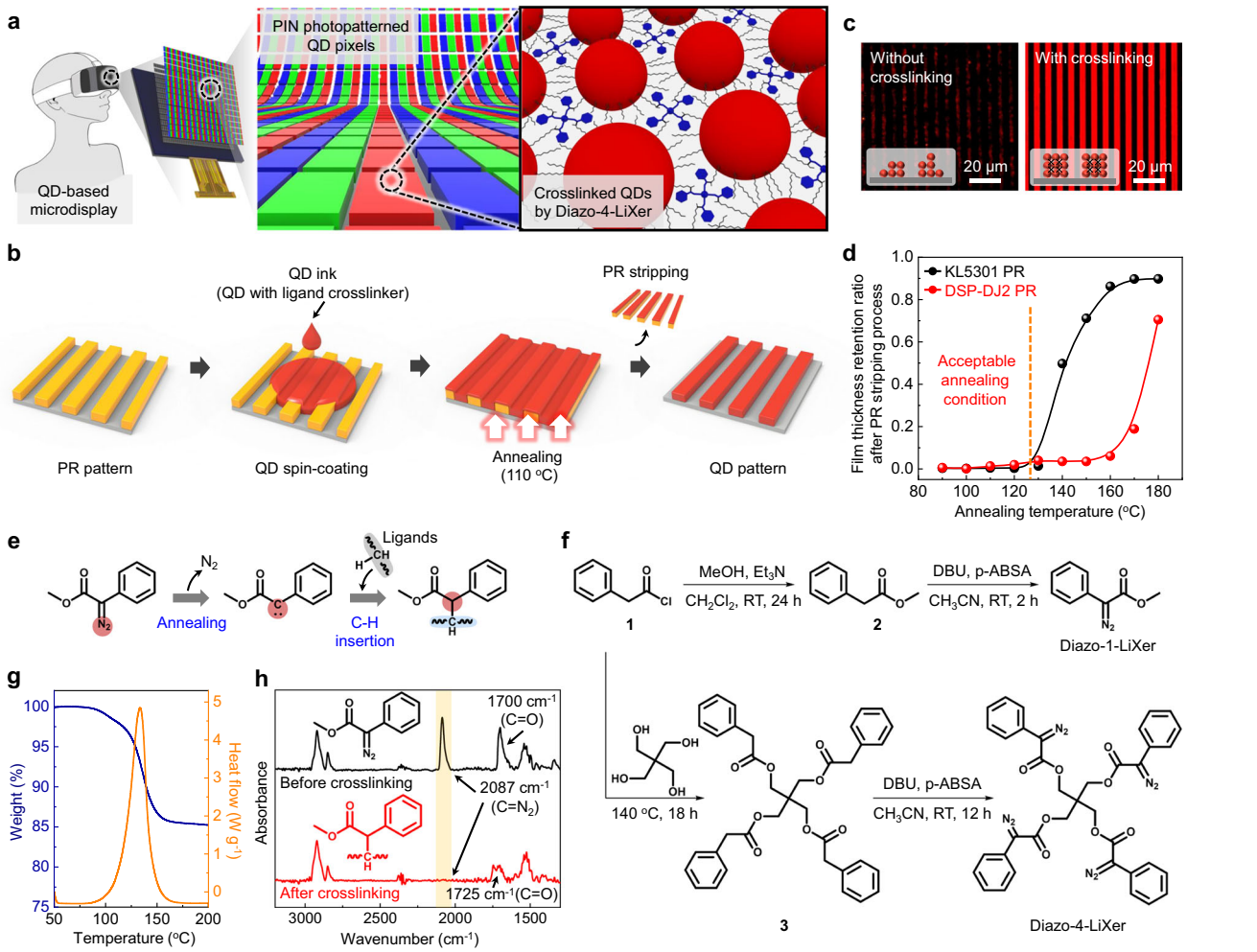

Fig. 1 | Concept of PIN photopatterning of quantum dots (QDs). a Schematic description of high-resolution QD display with RGB QD pixels formed using low-temperature-activatable ligand crosslinker. **b** Schematic illustrations of PIN photopatterning process using low-temperature-activatable ligand crosslinker. **c** Fluorescence microscope images of red-emitting QD patterns obtained through conventional photolithographic lift-off without crosslinking (left) and those obtained through PIN photopatterning with crosslinking (right). Red regions represent QD patterns. **d** Film thickness retention ratio of annealed KL5301/DSP-DJ2 PR films stripped using acetone. The region to the left of the orange dashed line indicates acceptable annealing conditions. **e** Scheme of thermally induced chemical reaction between Diazo-4-LiXer and the ligands of QDs. **f** Synthetic routes to Diazo-1-LiXer and Diazo-4-LiXer. **g** Thermogravimetric analysis (TGA) and differential scanning calorimetry (DSC) analysis of Diazo-4-LiXer. **h** Comparison of Fourier transform infrared (FT-IR) spectra of red-emitting CdSe/ZnSe/ZnS QD films blended with Diazo-4-LiXer before and after thermocrosslinking. Source data are provided as a Source Data file.

motion sickness or nausea that is often associated with immersive VR, AR, and MR experiences. Overall, there exists a significant demand for patterning technology to form high-resolution, high-fidelity red/green/blue (RGB) pixels.

Among emissive materials for displays, colloidal quantum dots (QDs) have been researched extensively in recent years owing to their potential for use in optoelectronic devices[5–12]. These materials exhibit intriguing physical characteristics, including tunable bandgap, narrow bandwidth, high luminous efficiency, and solution processability[13–17]. However, the development of a suitable patterning process for these solution-processed nanomaterials remains challenging. Photolithography has emerged as one of the most promising techniques among the various patterning methods available to date[18–23], especially because photolithography is already a fully established method for producing high-resolution patterns that fulfill industrial requirements[15,24]. In conventional photolithography, patterns are formed by physically or chemically etching the target materials along the features of the overlaid photoresist (PR) prepatterns[25–28]. In this process, the target materials must withstand harsh etching conditions while preserving their physical properties. However, the luminescence characteristics of nanostructured light-emitting materials such as QDs are likely to degrade during etching owing to the defects generated over their large surface areas. Recently, direct photopatterning has been exploited as a promising lithographic approach for forming patterns through selective chemical conversion of the target layer, followed by an appropriate developing step[24,29–43]. This approach excludes the etching step. However, the high-energy irradiation required for chemical conversion in direct photopatterning may potentially degrade the intrinsic luminescence properties of nanostructured light-emitting materials, especially QDs. Additionally, the fidelity of the QD patterns formed by direct photopatterning needs to be improved.

To avoid these challenges, an alternative approach called photolithographic lift-off patterning can be employed. With this approach, one can avoid subjecting the materials to harsh etching conditions and direct UV exposure by reordering the processing steps[44–47], as follows. First, sacrificial PR patterns are formed on a substrate. Next, the target materials are deposited onto the pre-patterned PR substrate. The underlying sacrificial PR patterns are then removed (or "lifted-off") by using a solvent, also called the stripping solvent. As the sacrificial PR

patterns are removed, the region of the target materials supported by the PR patterns is simultaneously stripped away. Eventually, patterns of target materials are formed. Despite these advantages, the process must be implemented carefully for patterning QDs. This is because QDs themselves, as well as their luminescent characteristics, may be susceptible to degradation during stripping of the sacrificial PR patterns. Therefore, strategies to prevent damage to the QD layer are crucial from the perspective of applying photolithographic lift-off patterning to these materials.

Herein, we report non-destructive photoresist-guided indirect (PIN) photopatterning of QDs by using a low-temperature-activatable ligand crosslinker called Diazo-4-LiXer (2,2-bis((2-diazo-2-phenylacetoxy)methyl)propane-1,3-diyl bis(2-diazo-2-phenylacetate)) that contains four diazo functional groups. Diazo-4-LiXer is structurally designed to induce carbene-mediated crosslinking between neighboring QDs. Such crosslinking is achieved using terminal diazo groups that are thermally activated to generate carbene intermediates at a low temperature of 110 °C, which leads to the occurrence of C-H insertion reactions with contacting aliphatic ligands[48–50]. PIN photopatterning can be applied universally for crosslinking various QD systems and even other nanocrystal systems encapsulated by aliphatic ligands. The low-temperature activation of Diazo-4-LiXer is critical for the success of PIN photopatterning because it creates a crosslinking condition that does not affect the structural properties of the underlying sacrificial PR layer, as well as the intrinsic physical properties of QDs (including their photoluminescence (PL) and electroluminescence (EL) characteristics). We demonstrate that μm-scale patterns of light-emitting QDs (CdSe/ZnSe/ZnS QDs, InP/ZnSeS QDs, and ZnSeTe/ZnSe/ZnS QDs), as well as combinations thereof, can be formed readily through PIN photopatterning by using Diazo-4-LiXer. Most importantly, the fidelity of the resulting patterns is the highest among the reported μm-scale QD patterns formed using photolithographic processes. This is attributed to the fact that the pre-formed PR patterns guide the structure of the QD patterns. In terms of the compatibility of PIN photopatterning with the apparatus used in the display industry and the non-destructive nature of the resulting high-fidelity QD patterns, the proposed method facilitates the realization of high-resolution QD-based optoelectronic devices.

Results

Photoresist-guided indirect photopatterning of QDs

PIN photopatterning of colloidal QDs was performed by following the steps illustrated in Fig. 1b. First, sacrificial PR patterns were formed onto a substrate by following conventional protocols, using KL5301 (from KemLab Inc.) and DSP-DJ2 (from Dongjin Semichem Co., Ltd.), both of which are commercially available positive PRs capable of forming thin patterns below 100 nm (the significance of PR pattern thickness is discussed below)[51]. A mixture of red-emitting CdSe/ZnSe/ZnS QDs and low-temperature-activatable ligand crosslinker (Diazo-4-LiXer) was spin-coated onto the substrate with sacrificial PR patterns. Subsequently, the resulting films were thermally annealed, which induced crosslinking between the ligands of neighboring QDs. Finally, by stripping the sacrificial PR patterns in a stripping solvent bath with ultrasonication, QD patterns (inverse of the PR patterns) were generated. Notably, PIN photopatterning is a modified photolithographic lift-off process tailored for solution-processed thin-films, in that it involves crosslinking of the target materials. Crosslinking the target materials endows the resulting patterns with chemical and physical stability against the stripping process of the sacrificial PR pre-patterns and the subsequent patterning process of neighboring patterns, which is also achieved using a solution process. Without crosslinking of the ligands, the QD films were removed easily upon exposure to the stripping solvent (Fig. 1c). To induce the ligand crosslinking reaction, we emphasize that either high-temperature (>140 °C) annealing or UV irradiation step should be avoided. This is because the chemical solubility of the underlying PR patterns can be altered by high-temperature annealing or UV irradiation. Figure 1d shows, for example, the ratio of thickness variation (referred to as the film thickness retention ratio) before and after soaking KL5301 and DSP-DJ2 PR films (annealed at different temperatures for 20 min) in a stripping solvent (i.e., acetone). In principle, the PR films should be completely removed by the stripping process, and, therefore, this ratio should equal zero. This was, in fact, only true for these PR films annealed at temperatures below 120 °C. In contrast, the PR films that were annealed at higher temperatures could not be removed completely under the same stripping condition, indicating that the solubility of the resulting PR films changed because of annealing at such temperatures.

Accordingly, we designed a low-temperature-activatable ligand crosslinker based on a diazo functional group, namely 2-diazo-2-phenylacetate. The diazo group can be activated thermally at temperatures below 120 °C to generate carbene species. These carbene species undergo a C-H insertion reaction with adjacent alkyl chains (Fig. 1e)[50]. Compared to the previously utilized fluorinated phenyl azide (FPA) compounds for crosslinking ligands of QDs through a nitrene-based C-H insertion reaction[30,34,52], the 2-diazo-2-phenylacetate compound used herein offers several advantages. First, even at the low annealing temperature of 110 °C, the crosslinking efficiency with alkyl chains of the diazo group approaches 76% (see "Methods" section, Fig. 1f, Supplementary Note 1, Supplementary Table 1, and Supplementary Figs. 1–24). Therefore, the QD films crosslinked using the diazo-based compound are compatible with PIN photopatterning using various PRs, including KL5301 and DSP-DJ2, the solubility of which does not change at such mild temperatures. Second, carbene-based crosslinking leads to better preservation of the luminescent properties of QDs compared to nitrene-based crosslinking[52]. Third, the carbene intermediate in this compound, which has a terminal phenyl group and an ester linkage to the core, exists in a secondary form. This steric environment likely reduces the accessibility of the reactive carbene to the inorganic QD surface, thereby suppressing undesired surface reactions and helping to preserve the luminescent properties of QDs[30]. Consequently, the resulting crosslinked QDs are expected to better retain their luminescent characteristics than those that use reactive intermediates in their primary forms.

By using the diazo functional group as the building block, we synthesized tetra-branched structured 2,2-bis((2-diazo-2-phenylacetoxy)methyl)propane-1,3-diyl bis(2-diazo-2-phenylacetate) (Diazo-4-LiXer). The chemical structure of Diazo-4-LiXer is illustrated in Fig. 1f, and its synthesis is described in the "Methods" section (Supplementary Figs. 25–30). The tetra-branched structure with four diazo moieties was used to increase the crosslinking efficiency of neighboring QDs[30,53]. The results of differential scanning calorimetry (DSC) and thermogravimetric analysis (TGA) confirmed that Diazo-4-LiXer was thermally activated while releasing four equivalents of N_2 (Fig. 1g). In this study, the carbenes, formed by releasing N_2, reacted with the ligands of neighboring QDs. The Fourier transform infrared (FT-IR) spectra depicted in Fig. 1h were obtained from CdSe/ZnSe/ZnS QD films before and after they were crosslinked using Diazo-4-LiXer at 110 °C for 20 min (the spectra obtained for different annealing times are shown in Supplementary Fig. 31). The peak at 2087 cm^{-1}, assigned to the C=N_2 stretching vibration of Diazo-4-LiXer, vanished after the thermal annealing step. In addition, the peak at 1700 cm^{-1}, assigned to the C = O stretching vibration of Diazo-4-LiXer, shifted to 1725 cm^{-1} after crosslinking of the ligands. This peak shift is attributed to the generation of new carbon-carbon bonds between the alkyl ligands of the QDs and Diazo-4-LiXer[48]. These results indicate that the QDs were crosslinked using Diazo-4-LiXer.

Fidelity analysis of QD patterns

After confirming the compliance of Diazo-4-LiXer in crosslinking the QD films, we performed PIN photopatterning. The fidelity of the

https://doi.org/10.1038/s41467-026-70770-z

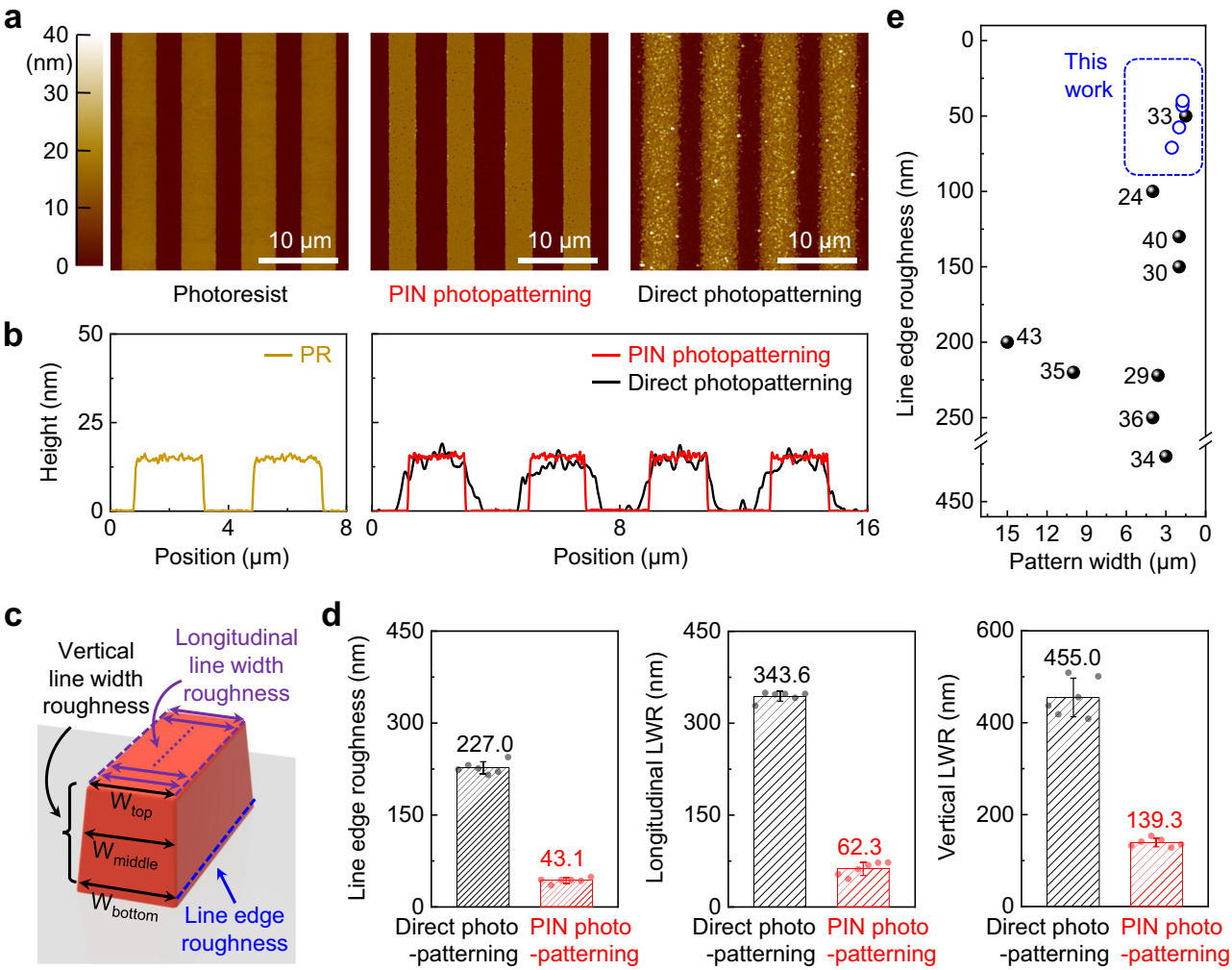

Fig. 2 | Fidelity of QD patterns produced using PIN photopatterning and direct photopatterning. a AFM images of 16-nm-thick DSP-DJ2 PR pattern and 16-nm-thick CdSe/ZnSe/ZnS QD patterns obtained using PIN photopatterning and direct photopatterning. **b** Comparison of height profiles of the patterns in (**a**). **c** Schematic illustration of a line QD pattern with physical parameters labeled, which include LER, l-LWR, and v-LWR. **d** Averaged values of LER, l-LWR, and v-LWR. LER, l-LWR, and v-LWR were determined as three times the standard deviation (3σ) of the edge position or line-width distributions. Data are presented as mean ± s.d. (standard deviation) from six independently prepared samples. Individual data points are overlaid. **e** Summary comparing the LER values reported in the literature with the values obtained in this study[24,29,30,33–36,40,43]. The results from this study are represented by the four blue open circles. From top to bottom, they correspond to: (1) Supplementary Fig. 37, (2) **a**, **b**, **d**, (3) Supplementary Fig. 39, and (4) Supplementary Fig. 38, respectively. Source data are provided as a Source Data file.

resulting QD patterns was compared to that of the QD patterns produced by direct photopatterning (which relies on a photoinduced change in solubility of the QD film, Supplementary Fig. 32)[30,34,35,50]. In fact, because the Diazo-4-LiXer can also undergo UV-induced carbene generation (365 nm, 4 mW cm^{-2}, 20 min), which leads to photocrosslinking of the QD ligands (Supplementary Fig. 33), this crosslinker can alternatively be used for the direct photopatterning of QD films. Notably, this UV exposure condition yielded a film thickness retention ratio above 0.9, indicating that the film was sufficiently crosslinked and that the processing condition was equivalent to the thermal process. Therefore, a direct comparative analysis of the QD patterns prepared using these two methods was possible. The CdSe/ZnSe/ZnS QD patterns prepared using the two photolithographic methods are compared in Fig. 2a, b by using atomic force microscopy (AFM) images and cross-sectional profiles, respectively. Here, the PIN photopatterning was done using DSP-DJ2 PR. These patterns were targeted to exhibit a width of 2 μm. Clearly, the PIN photopatterning yielded patterns with sharper edges compared to the alternative method. The quantitative features of the resulting patterns, such as line-edge roughness (LER), vertical line-width roughness (v-LWR, defined as the deviations of the line edges in the top, middle, and bottom of the pattern), and longitudinal line-width roughness (l-LWR, which denotes the variations in the pattern width along the longitudinal direction of the patterns), were characterized (Fig. 2c, d)[54]. The PIN photopatterning method produced QD patterns with a LER of 43.1 ± 4.4 nm, l-LWR of 62.3 ± 10.9 nm, and v-LWR of 139.3 ± 9.3 nm. Here, the values are the 3 sigma (3σ) value of the deviations, following the standard used in the PR community, which statistically indicates the range within which 99.7% of the measured deviations are expected to fall. Importantly, all these parameters were smaller than those achieved with the direct photopatterning process, where the LER was 227.0 ± 10.0 nm, l-LWR of 343.6 ± 7.9 nm, and v-LWR of 455.0 ± 42.0 nm. The improved pattern fidelity of the PIN photopatterns is attributed to the role of the preformed PR patterns, which provides structural guidance in defining the QD patterns (AFM images and cross-sectional profiles of the preformed PR patterns are shown in Fig. 2a, b, and Supplementary Figs. 34, 35). The improved pattern fidelity was additionally attributed to the use of stripping solvent (i.e., acetone) in shaping the QD patterns in the PIN photopatterning process (the stripping solvent should strip only the PR patterns and interact poorly with the target materials),

compared to the use of developing solvent (i.e., toluene) in direct photopatterning (the developing solvent is intended to remove uncrosslinked QDs from the film, but it can partially dissolve the loosely-crosslinked QDs in the crosslinked patterns owing to the favorable QD–solvent interaction by nature)[55]. The LER values of ≈40 nm (based on 3σ) achieved herein are the smallest among the photolithographically obtained QD patterns reported to date and represent a significant improvement over our previous direct photopatterning work when compared on an equivalent statistical basis (Fig. 2e and Supplementary Tables 2, 3). To highlight the novelty of PIN photopatterning using Diazo-4-LiXer, we constructed radar charts and the corresponding comparison table (Supplementary Fig. 36 and Supplementary Table 4). The radar charts clearly demonstrate that PIN photopatterning exhibits significantly improved performance compared to previously reported studies. Consistently, the improved pattern fidelity of the structures prepared using PIN photopatterning compared to that of the structures prepared using direct photopatterning was evident across different QD patterns in different dimensions prepared using different PRs (Supplementary Figs. 37–39).

We note the critical importance of precise control over the thickness of the pre-formed PR patterns to achieve high-fidelity QD patterns from PIN photopatterning process. In particular, the thickness of the pre-formed PR patterns should be comparable to that of the desired QD patterns. The results presented in Fig. 2a–d were obtained using 16-nm-thick PR patterns, which match well with the target thickness of the QD patterns (16 nm), considering their application as the emissive layer in EL devices. Here, this thickness was obtained either by using a commercial PR specifically designed for producing such ultrathin patterns (e.g., DSP-DJ2), or even by reactive-ion-etching thicker PR patterns (70 nm-thick KL5301) to the desired thickness. When thicker PR patterns (e.g., 70 nm patterns) were directly used instead, undesirable ear-structures were formed at the edge of the patterns owing to the capillary effect or undesired reactions crosslinking involving the photoactive compound in PR with QDs (Supplementary Note 2 and Supplementary Fig. 40).

Fabrication of mono- and multi-color QD patterns

Figure 3a, b shows sets of line and circle patterns of the red-emitting (R-) CdSe/ZnSe/ZnS QDs, green-emitting (G-) InP/ZnSeS QDs, and blue-emitting (B-) ZnSeTe/ZnSe/ZnS QDs. Patterns with 2 μm feature sizes could be achieved for these QDs. The minimal feature sizes of the QD patterns are constrained to the dimensions of the attainable PR patterns, which are determined by the type of PR and the specification of the UV irradiation system. For example, when an i-line stepper instead of a mask aligner was used, QD patterns with 0.8 μm feature sizes and a LER of 47.0 nm could be attained (see Supplementary Note 3 and Supplementary Fig. 41). The height profiles of these patterns, as obtained from AFM measurements, demonstrated their vertical sidewalls with no ear-structures (Fig. 3c, d). Importantly, because the resulting QD patterns were chemically crosslinked, they exhibited good structural tolerance against subsequent solution processes, such as the additional spin-coating of different QD layers or PR layers and the stripping process. Therefore, multi-color QD patterning could be realized by repeating the PIN photopatterning process as needed (Fig. 3e). In addition, previously deposited QD layers were protected from direct UV exposure during this process, ensuring the preservation of their performance (Supplementary Fig. 42). Figure 3f presents a fluorescence microscopy image of the RGB patterns formed by sequential deposition of R-, G-, and B-QDs. This image demonstrates that RGB QD patterns with pixel densities exceeding 4000 PPI can be formed using PIN photopatterning. More importantly, the morphology and height profiles of these patterns, as determined using AFM, indicate that the high fidelity of the patterns is well-preserved after multiple rounds of PIN photopatterning to form QD patterns of different colors (Fig. 3g). We also confirmed that QD patterns with complicated geometry could be obtained through PIN photopatterning (Supplementary Fig. 43). In addition, QD patterns with thickness above 2 μm could be prepared (Supplementary Fig. 44). Moreover, we confirmed that the Diazo-4-LiXer-based PIN photopatterning process can be applied universally to various nanocrystal systems (such as CuInS, InAs, and PbS QDs) so long as they are encapsulated with aliphatic ligands (Supplementary Fig. 45).

Luminescence characteristics of crosslinked QD films

Next, the luminescence characteristics of the crosslinked QD films were examined. Initially, the photoluminescence quantum yield (PLQY) and PL spectra of different QD films crosslinked using Diazo-4-LiXer were evaluated (Fig. 4a), and the data were plotted as a function of the film thickness retention ratio. This ratio, defined as the QD film thickness retained after soaking of the crosslinked QD films in toluene (which is the mother solvent used to cast the QD film), reflects the degree of film crosslinking. Increasing the amount of the crosslinker did not significantly deteriorate the PLQY. This contrasts with the gradual decrease in the PL characteristics upon the use of photoactivated nitrene-based LiXers[52]. The milder influence of crosslinking using Diazo-4-LiXer on the PL characteristics is attributed to the carbene-based reaction (compared to the nitrene-based reaction of the FPA-based crosslinkers) and the secondary reactive intermediate-based reaction (vs. primary reactive intermediate-based reaction), as discussed earlier when designing the crosslinker. Figure 4b depicts the transient PL decay profiles of the pristine and crosslinked R-, G-, and B-QD films. The R- and G-QD films were crosslinked using 5 wt.% Diazo-4-LiXer, and the B-QD films were crosslinked using 20 wt.% Diazo-4-LiXer. Crosslinking using Diazo-4-LiXer did not affect the luminescence characteristics of the QDs noticeably, which is consistent with the results presented in Fig. 4a. Figure 4c presents a comparison between the PLQYs of the QD films at different stages of the PIN photopatterning process, including post the thermocrosslinking of the films at 110 °C and post the stripping of the PR pre-patterns. The data were normalized against the PLQYs of the respective pristine QD films. No significant degradation in luminescence characteristics was observed, especially for the R- and G-QDs, even after completion of the entire PIN photopatterning process. A slight degradation in the luminescence characteristics of the B-QDs was observed, and it can potentially be alleviated by using more stable ligand-based blue-emitting QDs that will be developed in the future.

Additionally, the EL characteristics of the crosslinked QD layer were investigated using a light-emitting diode (LED) testbed containing the crosslinked R-QD emissive layer (Fig. 4d). The testbed device included a CdSe/ZnSe/ZnS QD layer as the emissive layer, a zinc magnesium oxide nanoparticle (ZnMgO NP) layer as the electron transport layer (ETL), and a 4,4-bis(*N*-carbazolyl)-1,1-biphenyl (CBP) layer as the hole transport layer (HTL) (Fig. 4d). The energy band diagram of the fabricated QD-LED is presented in Fig. 4e. For comparative analysis, three types of devices were fabricated: Device 1 with pristine red-emitting CdSe/ZnSe/ZnS QD layer (pristine), Device 2 with the same red-emitting QD layer crosslinked using 5 wt.% Diazo-4-LiXer (crosslinked), and Device 3 with the same red-emitting QD layer crosslinked using 5 wt.% Diazo-4-LiXer and underwent the entire PIN photopatterning process (including PR deposition, development, and stripping steps) (PIN photopatterned). It was found that the emission spectrum of Device 3 exhibited no difference compared to that of a reference device, i.e., Device 1, even after the EML underwent the entire PIN patterning process (Fig. 4f). The current density (J)-voltage (V)-luminance (L) profiles of these three devices (Fig. 4g), as well as the external quantum efficiency (EQE)-J profiles (Fig. 4h), were comparable. Likewise, crosslinking green and blue QDs did not degrade their EL characteristics (Supplementary Fig. 46). The well-preserved device characteristics can be attributed not only to the intrinsic PL properties of the QDs being maintained throughout the PIN photopatterning

https://doi.org/10.1038/s41467-026-70770-z

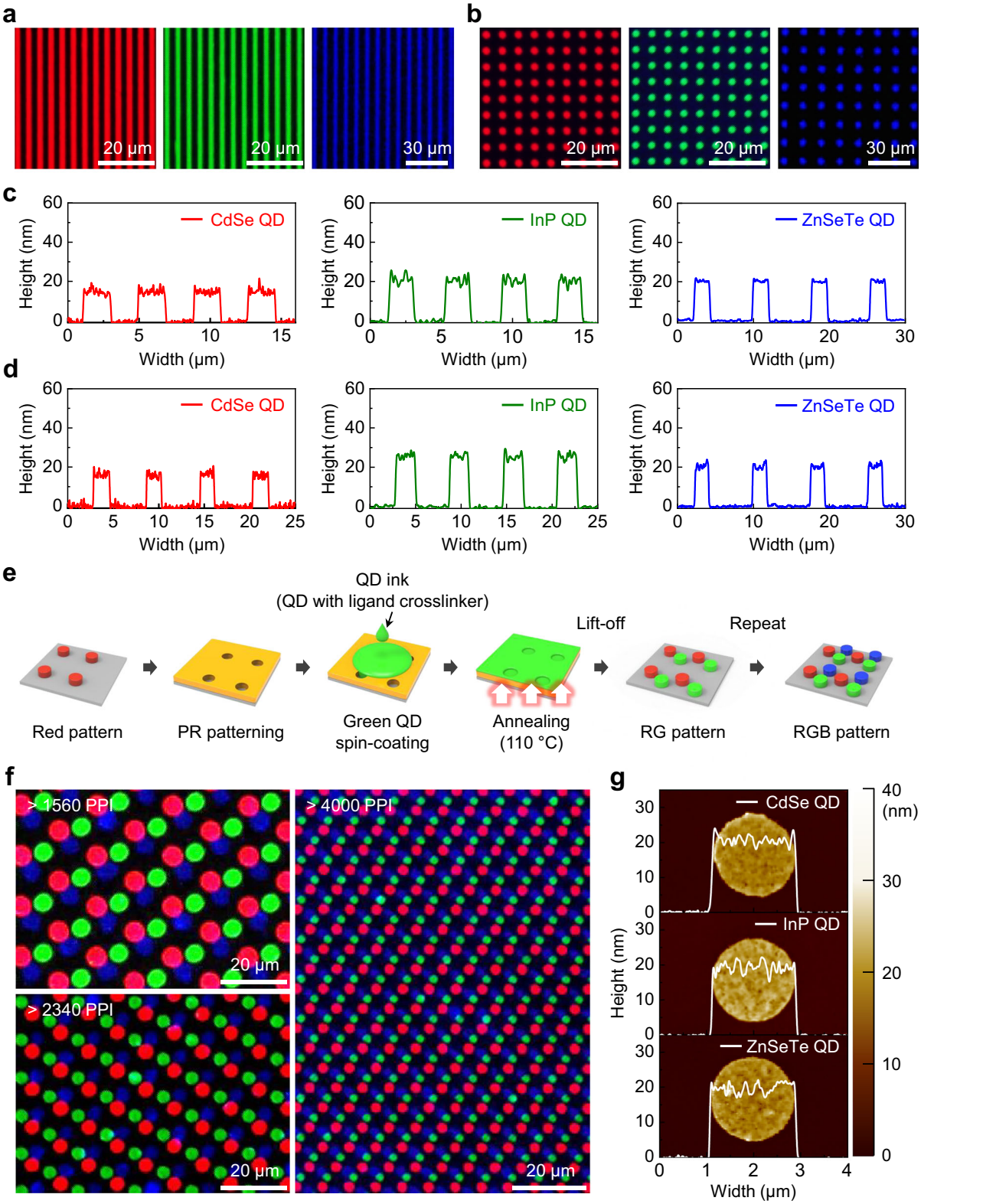

Fig. 3 | High-resolution and multi-colored QD patterns with high-fidelity obtained by PIN photopatterning. Fluorescence microscopy images of **a** line patterns (R- and G-QDs; width: 2 μm; spacing: 2 μm; B-QD; width: 2 μm; spacing: 6 μm) and **b** circle patterns (R- and G-QDs; width: 2 μm; spacing: 4 μm; B-QD; width: 2 μm; spacing: 6 μm) for R-, G-, and B-QDs obtained using the PIN photopatterning process. Height profiles of **c** lines patterns in (**a**), and **d** circle patterns in (**b**). **e** Schematic depicting the repeated PIN photopatterning processes applied to produce RGB QD patterns. **f** Fluorescence microscopy images of RGB patterns formed by the process described in (**e**). The subpixel dimensions are given as 6, 4, and 2 μm in diameter, and they are associated with the resolutions of approximately 1560, 2340, and 4000 PPI. **g** AFM images and height profiles of each of the R-, G-, and B-QD patterns (4000 PPI region). KL5301 PR was used for obtaining these patterns. Red, green, and blue colors denote CdSe, InP, and ZnSeTe QDs, respectively, in fluorescence images. Source data are provided as a Source Data file.

https://doi.org/10.1038/s41467-026-70770-z

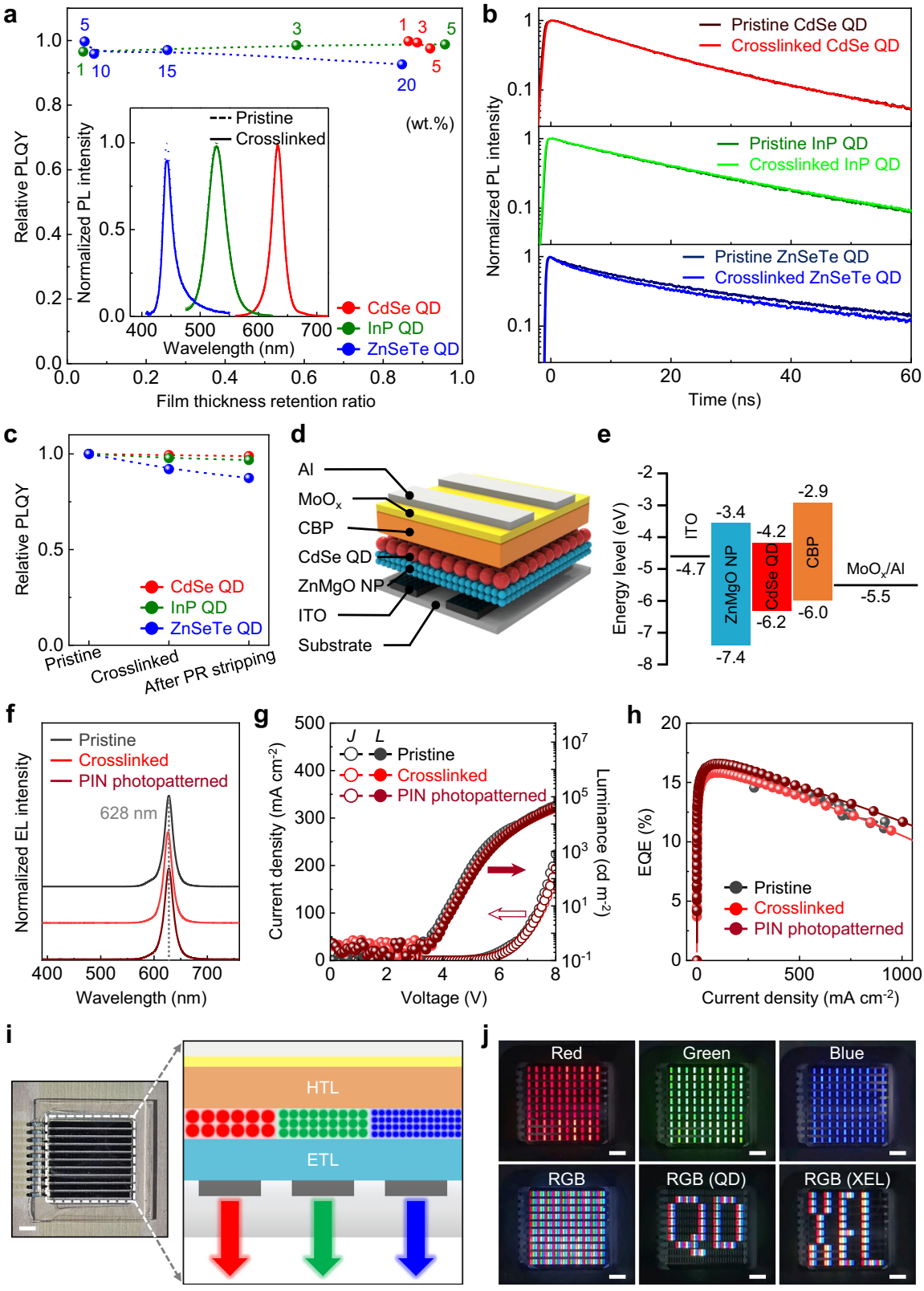

process (Fig. 4c), but also to the sufficient robustness of the underlying ZnMgO NP layer against the sequential processing steps involved in PIN photopatterning (Supplementary Fig. 47). These results confirm that Diazo-4-LiXer-mediated PIN photopatterning is a non-destructive process that preserves the optoelectronic properties of the QD layers. We further fabricate an RGB pixelated full-color display through consecutive PIN photopatterning of red-, green- and blue-emitting QDs. Step-by-step optical microscopy during the RGB fabrication cycles corroborates the robustness of this approach, revealing high-fidelity formation of sacrificial PR templates and QD patterns (Supplementary Fig. 48). Building on this reliable protocol, we demonstrate device-level applicability by realizing a 10 × 10 passive-matrix full-color RGB QD-LED array. Stable electroluminescence across driving modes, from monochromatic to full-color emission, underscores the scalability and

Fig. 4 | Luminescence characteristics of crosslinked QD films and full-color QD-LED arrays. a PLQY of the crosslinked QD film (relative to that of the pristine QD films) plotted as a function of the film thickness retention ratio for different QDs with different Diazo-4-LiXer loadings. The numbers in the figure indicate the weight percentage (wt.%) of Diazo-4-LiXer relative to those of the respective QDs. The inset data are the PL spectra of pristine (dashed) and crosslinked (solid) QD films. **b** Transient PL decay profiles of pristine and crosslinked R-, G-, and B-QD films. The R- and G-QD films were crosslinked using 5 wt.% Diazo-4-LiXer, and the B-QD films were crosslinked using 20 wt.% Diazo-4-LiXer. **c** Comparison of the PLQYs of QD films at different stages of the PIN photopatterning process, including that post thermocrosslinking at 110 °C and that post the PR stripping process. The data are normalized against the PLQYs of the respective pristine QD films. **d** Schematic illustration of the device structure, and **e** energy band diagram of the layers incorporated in the pristine/crosslinked R-QD EL devices. **f** EL spectra, **g** *J-V-L* characteristics, and **h** EQE-*J* characteristics of three different devices: Device 1 with pristine red-emitting CdSe/ZnSe/ZnS QD layer, Device 2 with the same red-emitting CdSe/ZnSe/ZnS QD layer crosslinked using 5 wt.% Diazo-4-LiXer, and Device 3 with the same red-emitting CdSe/ZnSe/ZnS QD layer crosslinked using 5 wt.% Diazo-4-LiXer and underwent the entire PIN photopatterning process (including PR deposition, development, and stripping steps). Scale bar, 200 μm. **i** Photograph of a fully fabricated 10 × 10 passive-matrix RGB QD-LED array. **j** Electroluminescent images showing red, green, blue, and full-color emission of the 10 × 10 RGB QD-LED array under different driving conditions. Scale bar, 2 mm. Source data are provided as a Source Data file.

versatility of this strategy for integrated high-resolution displays (Fig. 4i, j and Supplementary Movies 1, 2).

Discussion

We demonstrated non-destructive PIN photopatterning of QDs, enabling μms-scale QD patterns with structural fidelity using a low-temperature (110–120 °C)-activatable ligand crosslinker (Diazo-4-LiXer). The PIN photopatterning process consists of (1) lithographic formation of sacrificial PR patterns, (2) deposition of a QD film blended with Diazo-4-LiXer followed by mild annealing to induce thermo-crosslinking between the ligands of neighboring QDs, and (3) PR stripping that removes the sacrificial PR and leaves behind the crosslinked QD patterns on the substrate. The tetra-branched design of Diazo-4-LiXer, featuring four diazo functional groups, enables efficient carbene-mediated crosslinking of aliphatic QD ligands at 110 °C without compromising the structural integrity and stripability of the sacrificial PR layer as well as the intrinsic optoelectronic properties of the QD layer. By leveraging PR-guided pattern definition together with low-temperature ligand crosslinking, we achieved surpassing the attainable quality using direct photopatterning without compromising the luminescence characteristics. Notably, this approach simultaneously provides (1) optical/electrical non-destructiveness, (2) μm/sub-μm patterning capability, and (3) record-high fidelity metrics (e.g., LER on a consistent 3σ basis). Furthermore, we patterned device-relevant ultrathin QD emissive layers (16 nm), demonstrating compatibility with practical EL device stacks. We also achieved full-color RGB pattern integration with resolutions exceeding 4000 PPI by consecutively applying PIN photopatterning to R-, G-, and B-QDs, highlighting the robustness of the crosslinked QD patterns against repeated solution-based processing without direct UV exposure of previously patterned QD layers. Furthermore, we fabricated a 10 × 10 RGB QD-LED array, which exhibited stable EL under passive-matrix driving, providing integration-level validation of the process beyond single-pixel test devices. Overall, these results establish PIN photopatterning as an industry-compatible route for hyper-realistic QD displays.

Methods

Synthesis of crosslinkers and characterization

Materials. Deuterated chloroform ($CDCl_3$) for measurement of ^{1}H-NMR and ^{13}C-NMR spectra was purchased from Cambridge Isotope Laboratories (USA). 2,2-bis(hydroxymethyl)propane-1,3-diol (99%) and 2-phenylacetyl chloride (98%) were purchased from Alfa Aesar. 4-acetamidobenzenesulfonyl azide (p-ABSA, 97%), 2,3,4,6,7,8,9,10-octahydropyrimido[1,2-a]azepine (DBU, 98%), anhydrous acetonitrile (99.8%), anhydrous dodecane (≥99%), anhydrous methanol (99.8%), and anhydrous toluene (99.8%) were purchased from Sigma-Aldrich. Anhydrous dodecane for the C-H insertion reaction was degassed by three freeze-pump-thaw cycles. All other solvents were purchased from Daejung (Republic of Korea) and used without further purification.

Characterization. To identify the molecular structures of all the synthesized products, ^{1}H-NMR and ^{13}C-NMR spectra were measured by Agilent 400 MHz FT-NMR with $CDCl_3$ as a solvent. Mass spectra of synthetic materials were obtained by electrospray ionization-mass spectrometry (ESI) technique using AccuTOF 4G+ DART (JEOL, Japan). Fourier transform infrared spectroscopy (FT-IR) spectra of synthetic materials were obtained using Perkin Elmer Spectrum Two FT-IR Spectrometer.

C-H insertion reaction of Diazo-1-LiXer with dodecane. To verify that the diazo group undergoes thermolysis and C-H insertion at low temperatures, we synthesized a model compound of Diazo-1-LiXer (Fig. 1f) and monitored the C-H insertion reaction between a model compound of Diazo-1-LiXer (a crosslinkable unit of Diazo-4-LiXer) and neat dodecane (representing the aliphatic ligands of QDs). While the reaction using the model compound was conducted in the liquid phase, where the reactants have greater conformational freedom and larger diffusivity, we still consider that our model system remains highly relevant to the actual patterning chemistry. This is because once Diazo-4-LiXer is cast into a film with QDs, it must be surrounded completely by the alkyl chains of (i.e., QD ligands), just as in the neat solution model reaction. It is likely that the effective packing density of ligands (containing the reactant -CH_2- groups) surrounding Diazo-4-LiXer in the solid state might be higher than that of dodecane (containing the reactant -CH_2- groups) surrounding Diazo-1-LiXer in solution, due to the restricted molecular mobility in the solid phase. Considering that the diazo functional groups are still surrounded by an excess of reactive C-H bonds in the solid state, the fundamental crosslinking process would not be significantly different from a stoichiometric perspective, even in the solid-state patterning process. A similar approach using a model reaction was conducted in ref. 56, to analyze C-H insertion reactions on polymers such as PDMS and PS.

Synthesis of Diazo-1-LiXer

Methyl 2-phenylacetate, compound **2**: A mixture of phenylacetyl chloride (compound **1**, 200 mg, 1.47 mmol), triethylamine (1309 mg, 12.94 mmol) and anhydrous dichloromethane (10 mL) was stirred at RT for 10 min under argon atmosphere. Anhydrous methanol (415 mg, 12.94 mmol) was added dropwise to the solution. The reaction mixture was stirred at RT for 24 h. The resulting reaction mixture was extracted three times with dichloromethane (20 mL) and deionized water (20 mL). The combined organic layer was dried using anhydrous $MgSO_4$ and concentrated under reduced pressure. The crude product was purified by silica gel column chromatography (ethyl acetate: n-hexane, 1:10 v/v) to obtain compound **2** as a clear oil (843 mg, 87%). ^{1}H-NMR (400 MHz, $CDCl_3$) δ: 7.35–7.26 (m, 5H), 3.69 (s, 3H), 3.63 (s, 2H) (Supplementary Fig. 1).

Methyl 2-diazo-2-phenylacetate, Diazo-1-LiXer: A mixture of compound **2** (843 mg, 5.61 mmol), p-ABSA (2023 mg, 8.42 mmol), and anhydrous acetonitrile (20 mL) was stirred at RT for 10 min under an argon atmosphere. The DBU (1281 mg, 8.42 mmol) was added

dropwise to the solution. The reaction mixture was stirred at RT for 2 h. The resulting reaction mixture was extracted three times with dichloromethane (30 mL) and deionized water (30 mL). The combined organic layer was dried using anhydrous $MgSO_4$ and concentrated under reduced pressure. The crude product was purified by silica gel column chromatography (ethyl acetate: n-hexane, 1:10 v/v) to obtain Diazo-1-LiXer as an orange oil (534 mg, 54%). ^{1}H-NMR (400 MHz, $CDCl_3$) δ: 7.49–7.47 (d, J = 8.0 Hz, 2H), 7.41–7.37 (t, J = 8.0 Hz, 2H), 7.21–7.17 (t, J = 8.0 Hz, 1H), 3.87 (s, 3H) (Supplementary Fig. 2).

Experimental procedures of C-H insertion between Diazo-1-LiXer and dodecane

To a 20 mL vial with a magnetic bar, Diazo-1-LiXer (256.6 mg, 1.457 mmol) and anhydrous dodecane (6.5 mL, 4.872 g, 28.6 mmol) were added. The vial was tightly closed with a Teflon vial cap, and the gap between the vial and cap was sealed using Teflon tape. The entire vial was wrapped in aluminum foil to insulate and block out light. The reaction mixture was stirred at RT for 10 min. After 10 min, the vial was placed onto a hot plate, which was preheated to 150 °C and stirred for 200 min at 150 °C. For reaction monitoring using ^{1}H-NMR and FT-IR, 100 µL of the reaction mixture was collected every 20 min using a micropipette. For ^{1}H-NMR measurements, 50 µL of the collected reaction mixture was diluted in 600 µL of $CDCl_3$. FT-IR measurements were performed using a single drop of the collected reaction mixture. After 200 min, the remaining reaction mixture in the 20 mL vial was directly purified by silica gel column chromatography (ethyl acetate: n-hexane, 1:10 v/v) to remove residual dodecane and separate the C-H insertion products into three fractions. The obtained fractions (218 mg) were dried under vacuum. Finally, fraction A (130 mg, 0.408 mmol, 60%), fraction B (49 mg, 0.210 mmol, 22%), and fraction C (39 mg, 0.189 mmol, 18%) were obtained. The three fractions A, B, and C were analyzed using electrospray ionization-mass spectroscopy (ESI-MS) and ^{1}H-NMR (the corresponding data are shown in Supplementary Figs. 3–9). The mole calculations of each fraction are based on the assumption that the fractions A, B, and C are composed of the molecules that reacted one time, two times, and three times, respectively, with Diazo-1-LiXer, although each fraction is not completely pure. The reaction yield of Diazo-1-LiXer would be ≈55.4% (i.e., (0.408 + 0.210 + 0.189)/1.457). Based on this reaction yield of Diazo-1-LiXer, the crosslinking efficiency of Diazo-4-LiXer is 76.4%.

Synthesis of Diazo-4-LiXer

2,2-bis((2-phenylacetoxy)methyl)propane-1,3-diyl bis(2-phenylacetate), compound **3**: A mixture of phenylacetyl chloride (compound **1**, 1020 mg, 6.60 mmol) and 2,2-bis(hydroxymethyl)propane-1,3-diol (150 mg, 1.10 mmol) was stirred at 140 °C for 18 h under an argon atmosphere. After 18 h, the reaction mixture was cooled down to RT. The resulting reaction mixture was extracted three times with dichloromethane (30 mL) and deionized water (30 mL). The combined organic layer was dried using anhydrous $MgSO_4$ and concentrated under reduced pressure. The crude product was purified by silica gel column chromatography (ethyl acetate: n-hexane, 1:4 v/v) to obtain compound **3** as a white solid (483 mg, 72%). ^{1}H-NMR (400 MHz, $CDCl_3$) δ: 7.29–7.15 (m, 20H), 3.87 (s, 8H), 3.51 (s, 8H) (Supplementary Fig. 25). ^{13}C-NMR (100 MHz, $CDCl_3$) δ: 170.71, 133.46, 129.15, 128.67, 127.27, 62.06, 42.01, 41.10 (Supplementary Fig. 26). ESI-MS m/z Calcd: 631.2308 Found: 631.23 (M + Na) (Supplementary Fig. 27).

2,2-bis((2-diazo-2-phenylacetoxy)methyl)propane-1,3-diyl bis(2-diazo-2-phenylacetate), Diazo-4-LiXer: A mixture of compound **3** (400 mg, 0.66 mmol), p-ABSA (789 mg, 3.28 mmol) and anhydrous acetonitrile (10 mL) was stirred at RT for 10 min under an argon atmosphere. The DBU (670 mg, 4.40 mmol) was added dropwise to the solution. The reaction mixture was stirred at RT for 12 h. The resulting reaction mixture was extracted three times with dichloromethane (15 mL) and deionized water (15 mL). The combined organic layer was dried using anhydrous $MgSO_4$ and concentrated under reduced pressure. The crude product was purified by silica gel column chromatography (ethyl acetate: n-hexane, 1:5 v/v). Finally, the resulting product was recrystallized in $CHCl_3$/MeOH, and then filtered to obtain Diazo-4-LiXer as an orange solid (348 mg, 74%). ^{1}H-NMR (400 MHz, $CDCl_3$) δ: 7.43–7.34 (m, 16H), 7.21–7.16 (t, J = 8.0 Hz, 4H), 4.41 (s, 8H) (Supplementary Fig. 28). ^{13}C-NMR (100 MHz, $CDCl_3$) δ: 164.22, 129.00, 126.16, 124.81, 124.09, 62.67, 43.01 (Supplementary Fig. 29). ESI-MS m/z Calcd: 735.1928 Found: 735.19 (M+Na) (Supplementary Fig. 30).

Synthesis of quantum dots

Materials. Cadmium oxide (CdO, 99.998%), selenium (200 mesh, 99.999%), sulfur (trace metal basis, 99.98%), oleic acid (OA, 99%), 1-octadecene (ODE, 90%), tri-n-octylphosphine (TOP, 97%), and zinc acetate ($Zn(OAc)_2$, 99.99%) used for the synthesis of red-emitting QDs were purchased from Sigma-Aldrich. Green-emitting InP/ZnSeS QD were purchased from Uniam (Republic of Korea). Tellurium (Te, 99.999%) was purchased from Alfa Aesar. Oleic acid (OA, 99%), 1-octadecene (ODE, ≥90%), selenium (Se, 99.9%) and n-trioctylphosphine (TOP, 99%) used for the synthesis of blue-emitting QDs were purchased from Uniam. 1-dodecanethiol (DDT, ≥98 %), diphenylphosphine (DPP, 98%) and anhydrous ethanol (>99.8 %), and all solvents including toluene (anhydrous 99.8%), ethanol (anhydrous ≥99.5 %) were purchased from Sigma-Aldrich. All chemicals were used as received.

Synthesis of red-emitting CdSe/ZnSe/ZnS QDs. QD synthesis was performed using Schlenk line techniques under inert conditions. Zinc oleate (0.5 M, $Zn(OA)_2$) was prepared by heating 20 mmol of $Zn(OAc)_2$ with 12 mL of OA at 150 °C for 1 h, which was subsequently diluted with ODE to a total volume of 40 mL. Trioctylphosphine selenium (1 M, TOPSe) and trioctylphosphine sulfur (1 M, TOPS) were prepared by stirring 1 mmol of Se or S with 1 mL of TOP at RT overnight. For red-emitting CdSe/ZnSe/ZnS QDs (r = 3.0 nm, l = 5.0 nm, h = 2.0 nm), a mixture of 0.3 mmol of CdO, 1 mmol of OA, and 6 mL of ODE was loaded into a 3-neck flask and heated up to 300 °C under inert conditions to form a clear solution of $Cd(OA)_2$. Then, 0.5 mL of TOPSe (1 M) was rapidly injected into the reaction flask. After 3 min, 5 mL of Cd, Se stock solution in ODE was injected for the growth of CdSe cores. Next, 20 mL of $Zn(OA)_2$ (0.5 M) and 7 mL of TOPSe were added successively for the growth of the ZnSe shell. Finally, 10 mL of $Zn(OA)_2$ (0.5 M) and 5 mL of TOPS were added for the growth of the ZnS outer shell. The synthesized QDs were purified five times by the precipitation/redispersion (ethanol/toluene) method.

Synthesis of blue-emitting ZnSeTe/ZnSe/ZnS QDs. QD synthesis was performed using Schlenk line techniques under inert conditions. $Zn(OA)_2$ (0.5 M) stock solutions in ODE were prepared for cation precursors. TOPSe (2 M), trioctylphosphine telluride (0.05 M, TOPTe), and diphenylphosphine selenide (0.2 M, DPPSe) were prepared for anion precursors. For $Zn(OA)_2$ preparation, 50 mmol of $Zn(Ac)_2$ and 100 mmol of OA were mixed in a flask, degassed at 130 °C for 6 h, backfilled with N_2 gas, and then diluted to 0.5 M concentration with ODE. For TOPSe preparation, 100 mmol of Se powder was mixed with 50 mL of TOP at 160 °C for 5 h under inert conditions. The same procedure was adopted for preparing TOPTe. For DPPSe, 4 mmol of Se powder was reacted with 2 mL of DPP at 200 °C until complete reaction under inert conditions, and diluted to 0.2 M concentration with toluene at RT.

ZnSeTe/ZnSe/ZnS QDs (r = 1.8 nm, l = 1.8 nm, h = 0.6 nm) were synthesized following the previously reported method with minor modifications[57]. 1.2 mL of $Zn(OA)_2$ (0.5 M) and 10 mL of ODE were stirred and degassed at 110 °C in a 3-neck round flask. After 1 h of degassing to remove water and oxygen completely, it was backfilled with N_2 gas. Then, the mixture of 1.43 mL DPPSe (0.2 M) and 0.3 mL

TOPTe (0.05 M) was injected to synthesize $ZnSe_{0.95}Te_{0.05}$ cores at 230 °C and maintained for 30 min. The temperature was then raised to 300 °C for 15 min to ensure complete growth of $ZnSe_{0.95}Te_{0.05}$ cores (r = 1.8 nm). For further ZnSe shell growth on the core, 2/3.4/5 mL of $Zn(OA)_2$ (0.5 M) and 0.25/0.425/0.625 mL of TOPSe (2 M) were injected sequentially at 300 °C. Additional injection of 10 mL of $Zn(OA)_2$ (0.5 M) and 0.5 mL of DDT results in 0.6 nm-thick ZnS shell growth. The synthesized QDs were purified two times by the precipitation/redispersion (ethanol/toluene) method.

Materials for photopatterning of QDs and device fabrication

DSP-DJ2 PR was purchased from Dongjin Semichem Co., Ltd. (Republic of Korea). KL5301 and KL5315 PR were purchased from Kemlab Inc. (USA). AZ 300 MIF developer was purchased from AZ Electronic Materials (USA). ITO patterned glass substrates were purchased from AMG (Republic of Korea). 4,4-Bis(*N*-carbazolyl)-1,1-biphenyl (CBP, 99.9%) was purchased from OSM (Republic of Korea). Molybdenum oxide (MoO_3, 99.95%) and aluminum (Al, 99.999%) metal sources were purchased from Taewon Scientific Co. (TASCO, Republic of Korea).

Photolithography of PR and thickness control

All substrates were cleaned in an ultrasonic bath with acetone and isopropyl alcohol for 10 min each and then dried with a nitrogen gun. Selection criteria for compatible photoresists to our PIN photopatterning are provided in Supplementary Note 4. In the case of DSP- DJ2, PR was coated through a multi-step spin-coating process (500 rpm for 3 s, 2700 rpm for 25 s, and 500 rpm for 3 s), and the resulting film was soft-baked on a hot plate at 100 °C for 110 s. After soft-baking, PR films were irradiated for 2.1 s with a UV light source (365 nm, 9.8 mW cm^{-2}) through a photomask using a mask aligner (MDA-400LJ, MIDAS system) and were then hard-baked on a hot plate at 110 °C for 110 s. Hard-baked PR film was developed for 4 s in AZ 300 MIF developer diluted to 0.15 N (from 0.26 N tetramethylammonium hydroxide (TMAH) solution) and was rinsed with deionized water. The resulting thickness of the PR patterns was 16 nm.

In case of KL5301, PR was coated through a multi-step spin-coating process (500 rpm for 5 s, 4500 rpm for 40 s, and 2000 rpm for 2 s), and the resulting film was soft-baked on a hot plate at 105 °C for 1 min. After soft-baking, PR films were irradiated for 9 s with a UV light source (365 nm, 9.8 mW cm^{-2}) through a photomask using a mask aligner (MDA-400LJ, MIDAS system) and then were hard-baked on a hot plate at 115 °C for 1 min. Hard-baked PR film was developed in AZ 300 MIF developer for 4 s and was rinsed with deionized water. The resulting thickness of the PR patterns was 70 nm. To reduce the thickness, the patterns were exposed to reactive ion etching (RIE). RIE was performed over PR patterned substrates using Ar/O_2 mixed gas (40 cm^3 STP min^{-1} for Ar and 20 cm^3 STP min^{-1} for O_2 gas) with 50 W RF power. After the etching process, the resulting thickness of the PR patterns was reduced to 17 nm.

PIN photopatterning of QDs

To form 70 nm-thick CdSe/ZnSe/ZnS QD patterns, Diazo-4-LiXer (5 wt.% relative to QDs) was added to a solution of CdSe/ZnSe/ZnS QDs in toluene (55 mg mL^{-1}). The mixture solution was spin-coated (4000 rpm for 30 s) onto the PR pre-patterned substrate (PR thickness = 70 nm), and the resulting film was annealed at 110 °C for 20 min to induce crosslinking reaction. PR patterns were then stripped in an ultrasonic bath with acetone for 1 min and dried using a nitrogen gun.

To form 20-nm-thick QD patterns, Diazo-4-LiXer was added to QD solutions in toluene (15 mg mL^{-1}) in different loadings (5 wt.% for CdSe/ZnSe/ZnS and InP/ZnSeS QDs, and 20 wt.% for ZnSeTe/ZnSe/ZnS QD). The mixture solution was then spin-coated (4000 rpm for 30 s) onto the PR pre-patterned substrate (PR thickness = 17 nm), and the resulting film was annealed at 110 °C for 20 min to induce crosslinking reaction. PR patterns were then stripped in an ultrasonic bath with acetone for 1 min and dried using a nitrogen gun.

To create a multi-color pattern, different QDs were patterned in sequence. Initially, 20-nm-thick red-emitting CdSe/ZnSe/ZnS QDs were patterned through the method described above. Subsequently, PR pre-patterns were formed onto the substrate with red-emitting CdSe/ZnSe/ZnS QD patterns. Following, green-emitting InP/ZnSeS QDs were patterned through the method described above. By repeating the above process once again to PR pre-patterns and following the QD layer deposition and PIN photopatterning process, blue-emitting ZnSeTe/ZnSe/ZnS QD patterns could be formed. This process enabled the formation of multi-color QD patterns based on various types of QDs.

Direct photopatterning of QDs

Diazo-4-LiXer (5 wt.% relative to QDs) was added to red-emitting CdSe/ZnSe/ZnS QD solutions in toluene (70 nm-thick QD patterns, 60 mg mL^{-1}; 20-nm-thick QD patterns, 15 mg mL^{-1}). The mixture solution was spin-coated (70 nm-thick QD patterns, 2000 rpm for 60 s; 20-nm-thick QD patterns, 4000 rpm for 30 s) onto a substrate. The resulting film was crosslinked via UV (365 nm, 4 mW cm^{-2}, corresponding exposure 4.8 J cm^{-2}) through a photomask. Subsequently, the films were developed using fresh toluene solvent, which could selectively remove the uncrosslinked regimes of QD film and leave red-emitting CdSe/ZnSe/ZnS QD patterns.

Characterization

UV-visible absorption spectra were recorded using a V-770 UV-Vis-NIR spectrophotometer (JASCO, Japan). Crosslinking reaction in the QD film was verified by using an FT-IR4700 spectroscopy (JASCO) in an attenuated total reflection (ATR) mode using bare Si substrates. Surface morphology and height profile of the patterned QD and PR films were examined using a Park XE7 and an NX10 AFM system (Park Systems, Republic of Korea) under ambient conditions in a noncontact mode. For structural parameters analysis of the patterns including LER, l-LWR, and v-LWR, data were collected from 5 × 5 μm AFM images that were specifically captured with 1024-line scans, yielding an AFM image pixel size ≈5 nm. High-resolution single- and multi-color patterns of the PR and QDs were fabricated using an MDA-400LJ Mask Aligner (Midas system, Republic of Korea). PLQY of QD films is measured by Quantaurus-QY absolute PL quantum yield spectrometer (Hamamatsu Photonics, Japan) at 400 nm excitation wavelength. Time-resolved photoluminescence (TRPL) analysis was carried out using a time-correlated single photon counting (TCSPC) system. Fluorescence spectra were measured using an FS-2 fluorescence spectrometer (Scinco, USA) at 400 nm excitation wavelength. The electrical properties of the crosslinked QD films were examined by employing a Keithley 236 source measurement unit and a Keithley 2000 multimeter. These instruments were connected to calibrated Si photodiodes for accurate measurements.

Device fabrication

Pre-patterned ITO substrates were cleaned in an ultrasonic bath with deionized water, acetone, and isopropyl alcohol for 10 min each and were dried using a nitrogen gun. Entire QD-LEDs fabrication was carried out under inert conditions. 20 mg mL^{-1} of ZnMgO NPs were spin-coated onto a pre-patterned ITO substrate at 4000 rpm for 30 s, and the film was annealed at 80 °C for 30 min. 15 mg mL^{-1} of red-emitting CdSe/ZnSe/ZnS QDs (or 15 mg mL^{-1} of green-emtting InP/ZnSeS QDs, blue-emitting 10 mg mL^{-1} of ZnSeTe/ZnSe/ZnS QDs) added with 5 wt.% of Diazo-4-LiXer were then spin-coated onto ZnMgO NPs at 4000 rpm for 30 s and the resulting QD film was annealed at 110 °C for 20 min (in case of fabricating the 10 × 10 RGB pixel array, the red-, green-, and blue-emitting QD patterns were subsequently PIN photopatterned including three cycles of PR patterning, QD film casting, thermal

annealing, and the PR stripping steps). CBP (60 nm), MoO_x (10 nm) and Al (120 nm) were thermally deposited on the QD films under the pressure of ≈10^{-7} torr at deposition rates of 0.4–1.0, 0.1–0.2 and 1.0–2.0 Å s^{-1}, respectively. Note that the size of the EML pattern for Device 3 was equivalent to the size of the overlapping area between the top and bottom electrodes (1.4 mm by 1.4 mm), and therefore, the electrical leakage issue was not an issue, despite the use of patterned EML between non-patterned HTL and ETL.

Statistics and reproducibility

Unless otherwise indicated, data were obtained from at least three independently prepared samples. Optical microscopy and AFM images are representative of the results obtained from these independent samples.

Reporting summary

Further information on research design is available in the Nature Portfolio Reporting Summary linked to this article.

Data availability

The data that support the findings of this study are available from the corresponding authors upon request. Source data are provided with this paper.

References

1. Hsiang, E.-L. et al. AR/VR light engines: perspectives and challenges. *Adv. Opt. Photonics* **14**, 783–861 (2022).
2. Chen, Z., Yan, S. & Danesh, C. MicroLED technologies and applications: characteristics, fabrication, progress, and challenges. *J. Phys. D Appl. Phys.* **54**, 123001 (2021).
3. Park, S. Y., Lee, S., Yang, J. & Kang, M. S. Patterning quantum dots via photolithography: a review. *Adv. Mater.* **35**, 2300546 (2023).
4. Wu, M.-C., Chung, M.-C. & Wu, C.-Y. 3200 ppi matrix-addressable blue MicroLED display. *Micromachines* **13**, 1350 (2022).
5. García de Arquer, F. P. et al. Semiconductor quantum dots: technological progress and future challenges. *Science* **373**, eaaz8541 (2021).
6. Kagan, C. R., Lifshitz, E., Sargent, E. H. & Talapin, D. V. Building devices from colloidal quantum dots. *Science* **353**, aac5523 (2016).
7. Pietryga, J. M. et al. Spectroscopic and device aspects of nanocrystal quantum dots. *Chem. Rev.* **116**, 10513–10622 (2016).
8. Lim, J. et al. Perspective on synthesis, device structures, and printing processes for quantum dot displays. *Opt. Mater. Express* **2**, 594–628 (2012).
9. Cho, K.-S. et al. High-performance crosslinked colloidal quantum-dot light-emitting diodes. *Nat. Photonics* **3**, 341–345 (2009).
10. Dai, X., Deng, Y., Peng, X. & Jin, Y. Quantum-dot light-emitting diodes for large-area displays: towards the dawn of commercialization. *Adv. Mater.* **29**, 1607022 (2017).
11. Zhukov, A. E., Kryzhanovskaya, N. V., Moiseev, E. I. & Maximov, M. V. Quantum-dot microlasers based on whispering gallery mode resonators. *Light Sci. Appl.* **10**, 80 (2021).
12. Park, Y.-S., Roh, J., Diroll, B. T., Schaller, R. D. & Klimov, V. I. Colloidal quantum dot lasers. *Nat. Rev. Mater.* **6**, 382–401 (2021).
13. Alivisatos, A. P. Semiconductor clusters, nanocrystals, and quantum dots. *Science* **271**, 933–937 (1996).
14. Empedocles, S. A., Norris, D. J. & Bawendi, M. G. Photoluminescence spectroscopy of single CdSe nanocrystallite quantum dots. *Phys. Rev. Lett.* **77**, 3873–3876 (1996).
15. Jeong, B. G. et al. Colloidal spherical quantum wells with near-unity photoluminescence quantum yield and suppressed blinking. *ACS Nano* **10**, 9297–9305 (2016).
16. Ekimov, A. I., Efros, A. L. & Onushchenko, A. A. Quantum size effect in semiconductor microcrystals. *Solid State Commun.* **56**, 921–924 (1985).
17. Chen, O. et al. Compact high-quality CdSe–CdS core–shell nanocrystals with narrow emission linewidths and suppressed blinking. *Nat. Mater.* **12**, 445–451 (2013).
18. Kim, T.-H. et al. Full-colour quantum dot displays fabricated by transfer printing. *Nat. Photonics* **5**, 176–182 (2011).
19. Kim, B. H. et al. Multilayer transfer printing for pixelated, multicolor quantum dot light-emitting diodes. *ACS Nano* **10**, 4920–4925 (2016).
20. Yang, P., Zhang, L., Kang, D. J., Strahl, R. & Kraus, T. High-resolution inkjet printing of quantum dot light-emitting microdiode arrays. *Adv. Opt. Mater.* **8**, 1901429 (2020).
21. Liu, Y. et al. Efficient all-solution processed quantum dot light emitting diodes based on inkjet printing technique. *ACS Appl. Mater. Interfaces* **9**, 25506–25512 (2017).
22. Ali, A., Oh, S., Kim, W. & Oh, S. J. Advances in colloidal quantum dot-based displays for QLEDs and patterning applications. *Korean J. Chem. Eng.* **41**, 3545–3560 (2024).
23. Kim, Y., Yang, J. & Choi, M. K. Recent advances in transfer printing of colloidal quantum dots for high-resolution full color displays. *Korean J. Chem. Eng.* **41**, 3469–3482 (2024).
24. Fu, Z. et al. Direct photo-patterning of efficient and stable quantum dot light-emitting diodes via light-triggered, carbocation-enabled ligand stripping. *Nano Lett.* **23**, 2000–2008 (2023).
25. Hu, C. et al. The micropatterning of layers of colloidal quantum dots with inorganic ligands using selective wet etching. *Nanotechnology* **25**, 175302 (2014).
26. Kim, G.-H. et al. High-resolution colloidal quantum dot film photolithography via atomic layer deposition of ZnO. *ACS Appl. Mater. Interfaces* **13**, 43075–43084 (2021).
27. Shulga, A. G. et al. Patterned quantum dot photosensitive FETs for medium frequency optoelectronics. *Adv. Mater. Technol.* **4**, 1900054 (2019).
28. Lee, J. Y. et al. Nondestructive direct photolithography for patterning quantum dot films by atomic layer deposition of ZnO. *Adv. Mater. Interfaces* **9**, 2200835 (2022).
29. Hahm, D. et al. Direct patterning of colloidal quantum dots with adaptable dual-ligand surface. *Nat. Nanotechnol.* **17**, 952–958 (2022).
30. Yang, J. et al. Nondestructive photopatterning of heavy-metal-free quantum dots. *Adv. Mater.* **34**, 2205504 (2022).
31. Liu, D. et al. Direct optical patterning of perovskite nanocrystals with ligand cross-linkers. *Sci. Adv.* **8**, eabm8433 (2022).
32. Wang, Y., Fedin, I., Zhang, H. & Talapin, D. V. Direct optical lithography of functional inorganic nanomaterials. *Science* **357**, 385–388 (2017).
33. Cho, H. et al. Direct optical patterning of quantum dot light-emitting diodes via in situ ligand exchange. *Adv. Mater.* **32**, 2003805 (2020).
34. Yang, J. et al. High-resolution patterning of colloidal quantum dots via non-destructive, light-driven ligand crosslinking. *Nat. Commun.* **11**, 2874 (2020).
35. Maeng, S. et al. Direct photocatalytic patterning of colloidal emissive nanomaterials. *Sci. Adv.* **9**, eadi6950 (2023).
36. Lee, J. et al. Direct optical lithography of colloidal InP-based quantum dots with ligand pair treatment. *ACS Energy Lett.* **8**, 4210–4217 (2023).
37. Liu, D. et al. Nondestructive direct optical patterning of perovskite nanocrystals with carbene-based ligand cross-linkers. *ACS Nano* **18**, 6896–6907 (2024).
38. Qie, Y. et al. Ligand-nondestructive direct photolithography assisted by semiconductor polymer cross-linking for high-resolution quantum dot light-emitting diodes. *Nano Lett.* **24**, 1254–1260 (2024).
39. Yi, Y.-Q.-Q. et al. Nondestructive direct patterning of both hole transport and emissive layers for pixelated quantum-dot light-emitting diodes. *ACS Nano* **18**, 15915–15924 (2024).

40. Lee, J. et al. Photocleavable ligand-induced direct photolithography of InP-based quantum dots. *ACS Energy Lett.* **10**, 94–101 (2025).
41. Nie, Q. et al. Direct optical patterning of quantum dot light-emitting diodes based on ultrafast, low-energy, site-controlled click chemistry reaction. *Adv. Funct. Mater.* **35**, 2420829 (2025).
42. Seo, H. et al. Direct photolithography of colloidal InP-based quantum dots utilizing the photoligation method. *Chem. Mater.* **37**, 1424–1431 (2025).
43. Xiao, P. et al. Ligand-engineered direct optical lithography of nanocrystals with industrially compatible solvents. *ACS Nano* **19**, 14509–14520 (2025).
44. Park, J.-S. et al. Alternative patterning process for realization of large-area, full-color, active quantum dot display. *Nano Lett.* **16**, 6946–6953 (2016).
45. Lin, C. H. et al. Large-area lasing and multicolor perovskite quantum dot patterns. *Adv. Opt. Mater.* **6**, 1800474 (2018).
46. Mei, W. et al. High-resolution, full-color quantum dot light-emitting diode display fabricated via photolithography approach. *Nano Res.* **13**, 2485–2491 (2020).
47. Ji, T., Jin, S., Zhang, H., Chen, S. & Sun, X. W. Full color quantum dot light-emitting diodes patterned by photolithography technology. *J. Soc. Inf. Disp.* **26**, 121–127 (2018).
48. Yi, Y.-Q.-Q. et al. Molecular design of diazo compound for carbene-mediated cross-linking of hole-transport polymer in QLED with reduced energy barrier and improved charge balance. *ACS Appl. Mater. Interfaces* **14**, 39149–39158 (2022).
49. Yang, S. et al. Carbene-mediated polymer cross-linking with diazo compounds by C–H activation and insertion. *Macromolecules* **55**, 3423–3429 (2022).
50. Kost, J., Bleiziffer, A., Rusitov, D. & Rühe, J. Thermally induced cross-linking of polymers via C,H insertion cross-linking (CHic) under mild conditions. *J. Am. Chem. Soc.* **143**, 10108–10119 (2021).
51. Luo, C. et al. Review of recent advances in inorganic photoresists. *RSC Adv.* **10**, 8385–8395 (2020).
52. Lu, S. et al. Beyond a linker: the role of photochemistry of cross-linkers in the direct optical patterning of colloidal nanocrystals. *Angew. Chem. Int. Ed.* **61**, e202202633 (2022).
53. Kim, M. J. et al. Universal three-dimensional crosslinker for all-photopatterned electronics. *Nat. Commun.* **11**, 1520 (2020).
54. Levinson, H. J. *Principles of Lithography* (SPIE, 2010).
55. Park, S. Y. et al. Network of inorganic nanocrystals can swell: study of swelling-induced surface instability. *Small* **20**, 2306366 (2024).
56. Lepage, M. L. et al. A broadly applicable cross-linker for aliphatic polymers containing C–H bonds. *Science* **366**, 875–878 (2019).
57. Chang, J. H. et al. Pushing the band gap envelope of quasi-type II heterostructured nanocrystals to blue: ZnSe/ZnSe1-XTeX/ZnSe spherical quantum wells. *Energy Mater. Adv.* **2021**, 3245731 (2021).

Acknowledgements

This work was supported by the Samsung Research Funding & Incubation Center of Samsung Electronics under project number SRFC-MA1901-51. This work was also supported by the National Research Foundation of Korea (NRF) grants funded by the Ministry of Science, ICT, and Future Planning (2021R1A2C2008332 and RS-2024-00445116).

Author contributions

B.K., M.S.K., and C.K. conceptualized and supervised the project. H.H. and M.L. synthesized and characterized the crosslinker and organic molecules. H.K., C.H.L., S.R., J.K., S.Y.P., S.J.L., H.B., S.L., H.J., and Y.H.J. characterized crosslinked QD films and conducted the PIN photopatterning. J.S.P., H.J.L., J.W.P., J.S., W.K.B., and C.K. fabricated the electrical devices. H.K., H.H., and C.H.L. wrote the manuscript, and all authors reviewed the manuscript.

Competing interests

The authors declare no competing interests.

Additional information

Supplementary information The online version contains supplementary material available at https://doi.org/10.1038/s41467-026-70770-z.

Correspondence and requests for materials should be addressed to Chan-mo Kang, Moon Sung Kang or BongSoo Kim.

Peer review information *Nature Communications* thanks the anonymous reviewers for their contribution to the peer review of this work. A peer review file is available.

Reprints and permissions information is available at http://www.nature.com/reprints

Publisher's note Springer Nature remains neutral with regard to jurisdictional claims in published maps and institutional affiliations.

[1]Department of Chemical and Biomolecular Engineering, Sogang University, Seoul, Republic of Korea. [2]Department of Chemistry, Ulsan National Institute of Science and Technology (UNIST), Ulsan, Republic of Korea. [3]SKKU Advanced Institute of Nanotechnology (SAINT), Sungkyunkwan University, Suwon, Republic of Korea. [4]Reality Display Research Section, Electronics and Telecommunications Research Institute (ETRI), Daejeon, Republic of Korea. [5]Institute of Emergent Materials, Ricci Institute of Basic Science, Sogang University, Seoul, Republic of Korea. [6]Graduate School of Semiconductor Materials and Device Engineering, Ulsan National Institute of Science and Technology (UNIST), Ulsan, Republic of Korea. [7]Graduate School of Carbon Neutrality, Ulsan National Institute of Science and Technology (UNIST), Ulsan, Republic of Korea. [8]These authors contributed equally: Hyeokjun Kim, Hyobin Ham, Chang Hyeok Lim. ✉e-mail: nkcm@etri.re.kr; kangms@sogang.ac.kr; bongsoo@unist.ac.kr